

External field control of spin-dependent rotational decoherence of ultracold polar molecules

Alexander Petrov^{a,b}, Constantinos Makrides^{a,c}, and Svetlana Kotochigova^{a*}

^a*Department of Physics, Temple University, Philadelphia, PA 19122-6082, USA*

^b*St. Petersburg Nuclear Physics Institute, Gatchina, 188300; Division of Quantum Mechanics, St. Petersburg State University, 198904, Russia*

^c*Department of Physics and Astronomy, University of Toledo, Mailstop 111, Toledo, Ohio 43606, USA*

We determine trapping conditions for ultracold polar molecules, where pairs of internal states experience identical trapping potentials. Such conditions could ensure that detrimental effects of inevitable inhomogeneities across an ultracold sample are significantly reduced. In particular, we investigate the internal rovibronic and hyperfine quantum states of ultracold fermionic ground-state $^{40}\text{K}^{87}\text{Rb}$ polar molecules, when static magnetic, static electric, and trapping laser fields are simultaneously applied. Understanding the effect of changing the relative orientation or polarization of these three fields is of crucial importance for creation of decoherence-free subspaces built from two or more rovibronic states. Moreover, we evaluate the induced dipole moment of the molecule in the presence of these fields, which will allow control of interactions between molecules in different sites of an optical lattice and study the influence of the interaction anisotropy on the ability to entangle polar molecules.

PACS numbers:

I. INTRODUCTION

The experimental realization of a high phase-space density, quantum-degenerate gas of molecules, prepared in a single quantum state, [1–4] opens up exciting prospects for the ultimate control of their internal and external degrees of freedom. In addition, significant progress has been made in loading and manipulating diatomic molecular species in periodic optical potentials [5–7]. Polar molecules are of particular interest in such experiments as they have permanent electric dipole moments and therefore can interact via long-range tunable dipole-dipole interactions. Trapped in an optical lattice these molecules can form new types of highly-correlated quantum many-body states [8, 9]. Moreover, it has been proposed [10] that they can be quantum bits of a scalable quantum computer. Finally, ultracold molecules are also promising systems to perform high-precision measurements of a possible time variation of fundamental physical constants. In parallel, there is growing interest orienting (non-degenerate) polar molecules using intense pulsed AC fields sometimes combined with external static electric field [11–13]. The feasibility of orienting rotationally cold polar molecules in an external field has been demonstrated [14, 15].

Molecules have complex vibrational, rotational and hyperfine internal structure with many internal degrees of freedom [16, 17]. As was shown in recent experiments [5, 18], coherent control over internal quantum states of molecules plays a key role in manipulation of molecules with a long coherence time. An important property for controlling a molecule with light fields is its complex molecular dynamic polarizability $\alpha(h\nu, \vec{\epsilon})$ at radiation frequency ν and polarization $\vec{\epsilon}$ (h is Planck's constant). Multiplied with the laser intensity its real part deter-

mines the strength of a lattice potential. As different internal states have different polarizability their lattice depths or Stark shifts differ.

A second important property of polar molecules is its permanent dipole moment. Their rotational levels can be shifted and mixed with one another by applying an external electric field. In the presence of both a static external electric field and laser fields the ground state has an anisotropic polarizability [2]. The anisotropy of the dynamic polarizability of these levels manifests itself as a dependence on the relative orientation of the polarization of the trapping laser and the DC electric field. Finally, alkali-metal polar molecules have a nonzero nuclear electric-quadrupole and nuclear-magnetic moments of the constituent atoms. Then by applying a magnetic field, quadrupole and Zeeman interactions further mix states. The combined action of these three fields can be a powerful tool with which to manipulate and control ultracold molecules trapped in an optical potential.

For many applications of ultracold polar molecules it is advantageous or even required that two or more molecular rotational-hyperfine states have the same spatial trapping potentials. This is as a so-called “magic” condition. In atomic gasses magic conditions occur for specific off-resonant laser frequencies [19–21]. In molecular systems such frequencies exist when light resonant or nearly-resonant with molecular transitions is used [22]. Unwanted spontaneous emission can then lead to dephasing. Recent experimental and theoretical studies [18, 23] of ground-state polar molecules demonstrated that “magic” conditions can exist for off-resonant laser frequencies as long as the angle between the laser polarization and either an external magnetic or electric field is carefully controlled. In fact, Ref. [18] showed in measurements of the AC polarizability and the coherence time for microwave

transitions between rotational states that there exist a “magic” angle between the orientation of the polarization of the trapping light and a magnetic field. In this experiment no electric field was applied.

Here we extend the ideas of Ref. [16–18, 23] and perform a theoretical study of the internal rovibronic and hyperfine quantum states of the KRb molecules when simultaneously static magnetic and electric fields as well as nonresonant trapping lasers are applied. A schematic is shown in Fig. 1. The purpose of the study is to develop a quantitative model for energy levels, polarizability, and dipole moments for an efficient quantum coherent control of coupled rotational states. Our research is closely linked to ongoing experiments with ultracold KRb molecules [5, 6, 18]. Understanding the effect of changing the relative orientation or polarization of these three fields is of crucial importance for creation of decoherence-free subspaces built from two or more rovibronic and hyperfine states.

We also evaluate the imaginary part of the polarizability, due to spontaneous emission from excited electronic states. Here, the imaginary part is calculated assuming that excited vibrational levels have a linewidth evaluated by either using the linewidth of atomic K or Rb or using an optical-potential approach [24].

This paper is set up as follows. In Sec. II we construct the Hamiltonian of the rotating KRb molecule in the presence of the three external fields. We then present results of our calculation of the AC polarizability in Sec. III. The dipole-moment is calculated as a function of electric field in Sec. IV. We finish with a discussion of the imaginary part of the polarizability due to spontaneous emission of electronic excited states in Sec. V.

II. MOLECULAR HAMILTONIAN

We focus on rotational states of the lowest vibrational level of the singlet $X^1\Sigma^+$ ground-state potential of $^{40}\text{K}^{87}\text{Rb}$ in the presence of a magnetic and electric field as well as an AC trapping laser field. We denote the rotational states by the angular momentum quantum number N and its projection m_N onto the external magnetic field direction. Both K and Rb have nonzero nuclear spin, which align along the magnetic field, through the Zeeman interaction. Nuclear quadrupole interactions mix these nuclear hyperfine states with the rotation of the molecule. The relative directions of the fields are defined in Fig. 1. Throughout, angular momentum and tensor algebra is based on Ref. [25].

In practice we have determined the molecular polarizability and dipole moment starting from the molecular basis functions or channels

$$|N, m_N, m_a, m_b\rangle \equiv \phi_{v=0}(r) |X^1\Sigma^+\rangle Y_{Nm_N}(\alpha\beta) |i_a m_a, i_b m_b\rangle, \quad (1)$$

where $\phi_{v=0}(r)$ is the $v = 0$ radial vibrational wavefunction for interatomic separation r , which for the small N

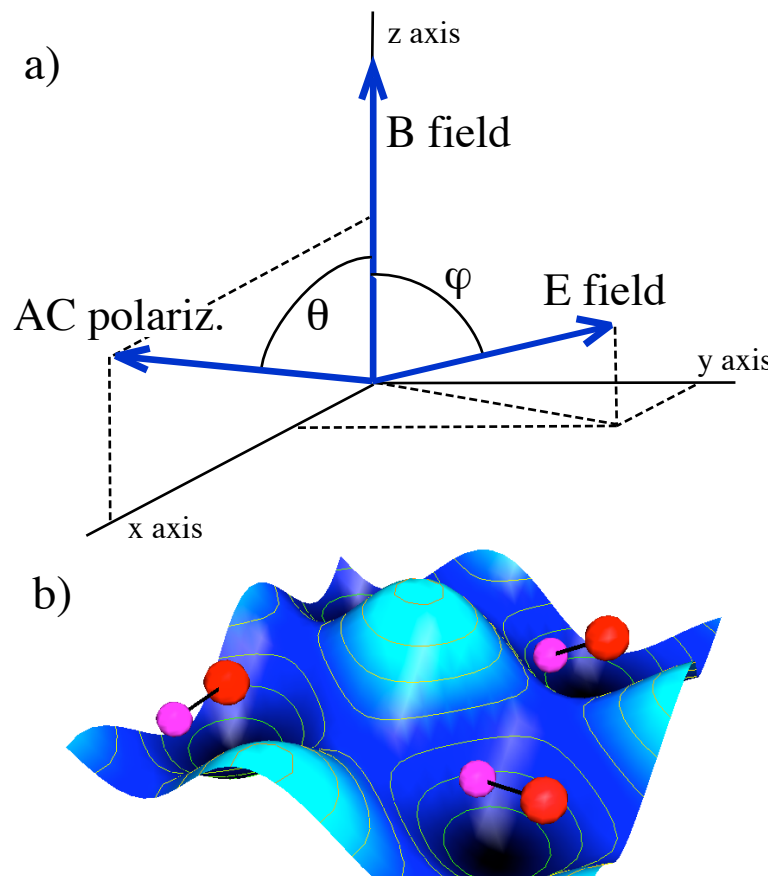


FIG. 1: (Color online) Panel a) shows the orientations of the static electric and magnetic fields as well as the AC polarization of the optical trapping laser. Without loss of generality, we assume that the magnetic field, \vec{B} , is directed along the z axis, while the polarization $\vec{\epsilon}$ of the laser lies in the x - z plane. The electric field \vec{E} can be in any direction. Only two of the three angles that uniquely specify the relative orientations are indicated. Panel b) shows a cartoon of polar molecules held in an optical lattice potential with polarization $\vec{\epsilon}$.

studied here is to good approximation independent of N , and $|X^1\Sigma^+\rangle$ is the electron wavefunction with projections defined along the internuclear axis. The spherical harmonic $Y_{Nm_N}(\alpha\beta)$ describes the rotational wavefunction of our Σ molecule. The angles α and β and projection m_N are defined with respect to the magnetic field direction. The nuclear spins \vec{i}_a and \vec{i}_b for atom a and b have projections m_a and m_b onto the magnetic field. For $^{40}\text{K}^{87}\text{Rb}$ there are 144 channels $|N, m_N, m_a, m_b\rangle$ with $N = 0$ and 1. The degeneracy of states with projections m_N for the same N is lifted by the interaction between the nuclear quadrupole moment and the rotation of the molecule [5, 18]. Here we focus on hyperfine states whose dominant nuclear spin character is $m_a = -4, m_b = 1/2$ for ^{40}K and ^{87}Rb , respectively. These states were selected for the experimental measurements dynamic polarizability in the ground state KRb molecule [18].

The effective Hamiltonian for the $v = 0$ rotational-hyperfine levels is given by

$$H = H_{rot} + H_Z + H_E + H_Q + H_{pol}, \quad (2)$$

and

$$H_{rot} = B_v \vec{N}^2 \quad (3)$$

$$H_Z = - \sum_{k=a,b} \mu_k \vec{i}_k \cdot \vec{B} \quad (4)$$

$$H_E = -\vec{d} \cdot \vec{E} \quad (5)$$

$$H_Q = \sum_{k=a,b} Q_k C_2(\alpha\beta) \cdot T_2(\vec{i}_k, \vec{i}_k) \quad (6)$$

$$H_{pol} = -(\alpha_{\parallel} \mathcal{O}_{\parallel} + \alpha_{\perp} \mathcal{O}_{\perp}) I, \quad (7)$$

where H_{rot} is the rotational Hamiltonian with vibrationally-averaged rotational constant $B_v = \int_0^{\infty} dr \phi_v(r) \hbar^2 / (2\mu r^2) \phi_v(r)$, where μ is the reduced mass and $\hbar = h/2\pi$. The matrix operator of H_{rot} is diagonal with our basis functions. For the KRb dimer the energy spacing Δ between vibrational levels $v = 0$ and $v = 1$ is on the order of $\Delta/h = 1500$ GHz, while $B_v/h = 1.1139$ GHz for $v = 0$ [1].

The next term in the Hamiltonian is the nuclear Zeeman interaction H_Z for each atom, where μ_k is the nuclear magneton of atom k [26] and \vec{B} is the magnetic field and only affects the nuclear spins. This contribution is followed by the electric-dipole interaction H_E , which describes the effect of a static electric field \vec{E} and contains the vibrationally-averaged molecular dipole moment operator \vec{d} . Matrix elements of H_E follow the realization that H_E can equivalently be written as $-d_0 \sum_{q=-1}^1 (-1)^q C_{1q}(\alpha\beta) E_q$, where $d_0 = \int_0^{\infty} dr \phi_{v=0}(r) \mathcal{D}(r) \phi_{v=0}(r)$ and $\mathcal{D}(r)$ is the r -dependent permanent electric dipole moment of the $X^1\Sigma^+$ potential. Moreover, E_q are the rank-1 spherical components of \vec{E} and $C_{lm}(\alpha\beta) = \sqrt{4\pi/(2l+1)} Y_{lm}(\alpha\beta)$ is a spherical harmonic of rank l . It follows that matrix elements are nonzero when $N+1+N'$ is even. We use $d_{v=0} = 0.223 ea_0$ for KRb, where e is the electron charge and $a_0 = 0.05292$ nm is the Bohr radius. The value is consistent with the result of Ref. [1].

Equation 2 also includes the nuclear quadrupole interaction H_Q for each atom. It has coupling constants Q_k and couples the nuclear spin to rotational states. Here, $T_{2m}(\vec{i}_k, \vec{i}_k)$ is a rank-2 tensor constructed from spin \vec{i}_k . For KRb the two quadrupole parameters Q_k were first determined in Ref. [5] based on measurements of transition energies between sub-levels of the $N = 0$ and $N = 1$ states. We use the more recent values $Q_K/h = 0.452$ MHz and $Q_{Rb}/h = -1.308$ MHz from [18].

Finally, we must include a term that describes the “reduced” AC Stark shift H_{pol} with strengths α_{\parallel} and α_{\perp} , rank-2 tensor operators \mathcal{O}_{\parallel} and \mathcal{O}_{\perp} , and laser intensity I [23]. This Stark shift is “reduced” in the sense that it is the Stark shift of the molecule when the other terms

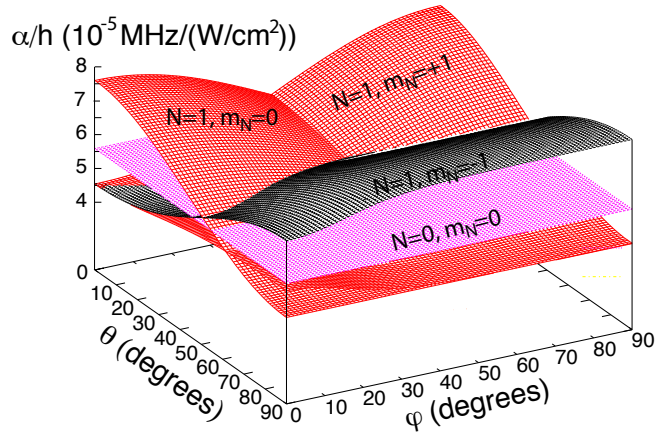


FIG. 2: (Color online) Polarizability of four rotational-hyperfine states of the $v = 0$ vibrational level of the $X^1\Sigma^+$ potential of KRb as a function of angle θ between the polarization of the dipole-trap laser and magnetic field, and as a function of angle φ between the static electric and magnetic fields. The electric field lies in the y - z plane as defined in Fig. 1. The magnetic field strength is $B = 545.9$ G, the electric field strength $E = 1$ kV/cm, and the laser at 1063 nm has an intensity of $I = 2.35$ W/cm². The four surfaces are labeled by rotational levels $|N, m_N\rangle = |0, 0\rangle$, $|1, 0\rangle$, $|1, -1\rangle$, and $|1, +1\rangle$, respectively. Their nuclear spin wavefunction is $m_a = -4$ and $m_b = 1/2$ for potassium and rubidium, respectively.

in our Hamiltonian are ignored and the “reduced” polarizabilities α_{\parallel} and α_{\perp} only depend on the laser frequency. In fact, these two polarizabilities can be expressed in terms of a sum over ro-vibrational states of all excited $^1\Sigma^+$ and $^1\Pi$ electronic potentials, respectively. The operators \mathcal{O}_{\parallel} and \mathcal{O}_{\perp} capture all dependence on light polarization and rotational angular momentum \vec{N} . For a 1063 nm laser $\alpha_{\parallel}/h = 10.0 \times 10^{-5}$ MHz/(W/cm²) and $\alpha_{\perp}/h = 3.3 \times 10^{-5}$ MHz/(W/cm²) measured in Ref. [18].

We find eigen-energies of this Hamiltonian by diagonalization, including rotational levels $N \leq 20$, and analyze its eigenfunctions to connect to states that have been observed experimentally. Eigenstates can be identified by the channel state with the largest contribution, although for field strengths and laser intensities accessible in ultracold molecular experiments we expect that the eigenstates can be severely mixed. The polarizability of eigenstate j with energy $\mathcal{E}_j(I, E)$ is defined as the derivative $\alpha_j = -d\mathcal{E}_j/dI$, while the dipole moment of state j is $\vec{d}_j = -d\mathcal{E}_j/d\vec{E}$. In this paper these two quantities are studied as a function of angles θ and φ , defined in Fig. 1a, magnetic field strength B , electric field strength E , and intensity I of the trapping laser field.

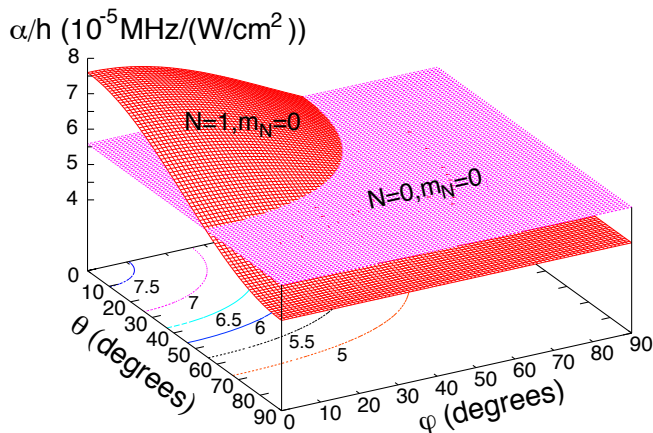


FIG. 3: (Color online) Polarizability of two $m_N = 0$ rotational-hyperfine states of the $v = 0$ vibrational level of the $X^1\Sigma^+$ potential of KRb as a function of angles θ and φ . Six contours of constant polarizability of the $|N = 1, m_N = 0\rangle$ state are plotted as well. The polarizability of the $|N = 0, m_N = 0\rangle$ state is independent of the two angles. The contour marked by 5.5 approximately corresponds to “magic” conditions for the two $m_N = 0$ rotational-hyperfine states. Parameters and remaining orientation are as for Fig. 2.

III. REAL PART OF POLARIZABILITY

In this section we present results for the dynamic polarizability of the $N = 0$ and $N = 1$ rotational levels of the $v = 0$ vibrational level of the ground $X^1\Sigma^+$ state of $^{40}\text{K}^{87}\text{Rb}$. The molecules are placed in an optical dipole trap created from a focussed laser with a wavelength of 1063 nm. An external magnetic field of $B = 545.9$ G and a static electric field are also present. The values of the fields and laser intensities are based on recent measurements with ultra-cold KRb molecules [18].

Figure 2 shows the polarizability as a function of θ and φ based on the Hamiltonian in Eq. 2 and the geometry defined in Fig. 1a for four rotational-hyperfine states. The laser intensity $I = 2.35$ kW/cm² and the electric field strength $E = 1$ kV/cm. We focus on the four states that have a predominant $|N, m_N, m_a, m_b\rangle = |0, 0, -4, 1/2\rangle$, $|1, 0, -4, 1/2\rangle$, and $|1, \pm 1, -4, 1/2\rangle$ character as they are of experimental interest. We observe that the polarizabilities of $N=1$ states change noticeably when going from small to and large values of the angles, while that for $|0, 0, -4, 1/2\rangle$ does not change for any angle. Figure 2 shows that the polarizabilities of hyperfine levels coincide for many values of θ and ϕ angles. Crossings of polarizabilities correspond to the so-called “magic” angles θ and φ , where the differential Stark shift for two or more states is zero. In fact, Fig. 3 shows that the magic angles between the states $|0, 0, -4, 1/2\rangle$ and $|1, 0, -4, 1/2\rangle$ form a nearly circular, elliptical curve that starts at $\theta = 57$ degrees and $\varphi = 0$ degrees.

Figures 4 and 5 show cuts through the surfaces de-

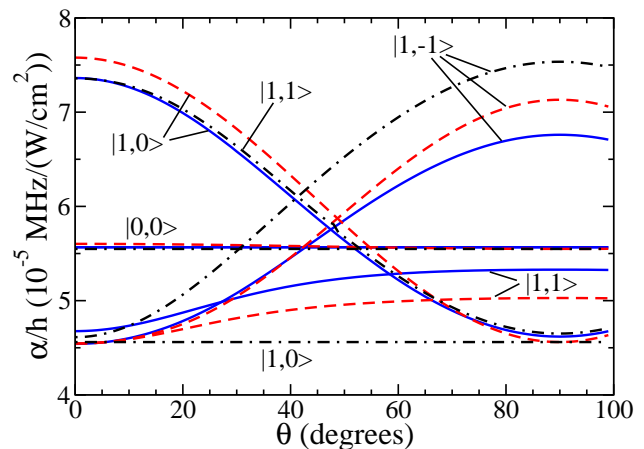


FIG. 4: (Color online) Polarizability of four rotational-hyperfine states of the $v = 0$ vibrational level of the $X^1\Sigma^+$ potential of KRb as a function of angle θ between the polarization of the dipole-trap laser for three configurations of the electric field. The solid blue lines are for zero electric field. They were previously published in Ref. [18]. The red dashed lines are for an electric field with a strength of 1 kV/cm oriented parallel to the magnetic field ($\varphi = 0^\circ$), while the dash-dotted black lines are for $E = 1$ kV/cm oriented in the y - z plane but perpendicular to the magnetic field ($\varphi = 90^\circ$). Remaining parameters and nuclear hyperfine states are as for Fig. 2 and note that the x axis extends to 100° .

picted in Figs. 2 and 3 in order to facilitate a quantitative comparison. Figure 4 shows the polarizability for four rotational-hyperfine states as a function of θ without applied electric field as well as for $E = 1$ kV/cm oriented either parallel ($\varphi = 0^\circ$) and perpendicular ($\varphi = 90^\circ$) to the magnetic field. The curves for zero electric field and that for $E = 1$ kV/cm with $\varphi = 0^\circ$ are similar in shape and predict “magic” conditions between $\theta = 50^\circ$ and 60° . The polarizability for the $|1, 0, -4, 1/2\rangle$ state decreases by as much as a factor of two for increasing θ . On the other hand, for $E = 1$ kV/cm and $\varphi = 90^\circ$ the polarizabilities of $|0, 0, -4, 1/2\rangle$ and $|1, 0, -4, 1/2\rangle$ do not cross. In fact, the polarizability of the $|1, 0, -4, 1/2\rangle$ state is nearly independent of angle θ , while that for the $|1, 1, -4, 1/2\rangle$ state now decreases by a factor of two for increasing θ .

Figure 5 shows the polarizability for the same four states as a function of φ for one value of θ and $E = 1$ kV/cm. For this value of θ the magic condition between states $|0, 0, -4, 1/2\rangle$ and $|1, 0, -4, 1/2\rangle$ occurs at the relatively-small angle $\varphi = 23^\circ$. On the other hand, the polarizability of the $|1, -1, -4, 1/2\rangle$ state does not coincide with that of the $|0, 0, -4, 1/2\rangle$ state at any angle φ .

Our analyses shows that for a trapping laser light at 1063 nm and external electric field strengths of 1 kV/cm only a few low-lying rotational states are mixed. The near infrared laser frequency is detuned away from resonances with rovibrational levels of the electronically ex-

cited potentials. As a result, corrections to the polarizability from the level shifts due to the static electric and magnetic field are significantly suppressed.

IV. INDUCED DIPOLE MOMENT

Figure 6 shows the induced dipole moment of four rotational-hyperfine levels along the electric field direction as a function of the electric field strength E . We assume an angle $\theta = 51^\circ$ between the magnetic field and the laser polarization and angle $\varphi = 23^\circ$ between the electric and magnetic fields, to ensure that the $|N, m_N\rangle = |0, 0\rangle$ and $|1, 0\rangle$ states have the same polarizability at $E = 1$ kV/cm. The nuclear spin state is $m_a = -4$ and $m_b = 1/2$. For $E < 7$ kV/cm the dipole moment of the $|1, 0\rangle$ state decreases with E and is negative. On the other hand, dipole moment of $|0, 0\rangle$ and $|1, \pm 1\rangle$ states always increase with E and are positive. For $E \gg 10$ kV/cm the induced dipole moments of all four rotational-hyperfine levels converge to $d_0 = 0.223 ea_0$. From results not shown here, we find that the induced dipole moment is aligned along the direction of the electric field, $\vec{d}_j \propto \vec{E}$, and that the magic conditions are nearly independent of electric field strength. Both observations follow from the fact that $m_a = -4$ and $m_b = 1/2$ are approximately good quantum numbers and that, for fields shown in Fig. 6, H_E is much larger than H_Z and H_Q . The coupling between rotational and nuclear spin states is weak. Then, for small electric field strengths, the four \vec{d}_j follow the

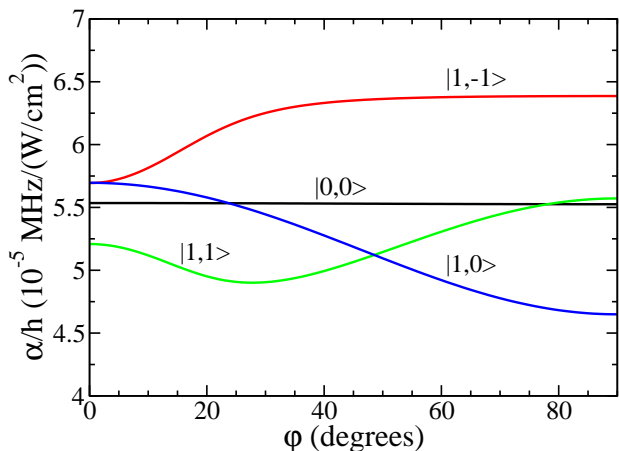


FIG. 5: (Color online) Polarizability of four rotational-hyperfine states of the lowest vibrational level of the $X^1\Sigma^+$ potential of KRb as a function of angle φ between the electric field and the magnetic field and $\theta = 51$ degrees. For this value of θ the “magic” angle φ is 23 degrees. All other parameters are the same as for Fig. 2.

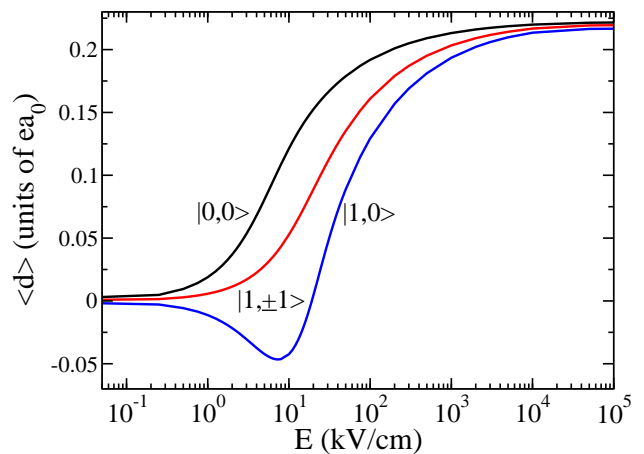


FIG. 6: (Color online) The induced dipole moment of the lowest rotational levels of the $v = 0$ vibrational level of the $X^1\Sigma^+$ potential of $^{40}\text{K}^{87}\text{Rb}$ as a function of external electric field strength E . The angles θ and φ are 51 degrees and 23 degrees, respectively. The laser intensity, remaining orientation, and magnetic field strength are the same as for Fig. 2.

second-order perturbation theory expressions

$$\begin{aligned} \vec{d}_{N,m_N=0,0} &= 2 \frac{d_0^2 |\langle 0,0 | C_{10} | 1,0 \rangle|^2}{2B_v} \vec{E}; \\ \vec{d}_{1,0} &= 2 \left[-\frac{d_0^2 |\langle 0,0 | C_{10} | 1,0 \rangle|^2}{2B_v} + \frac{d_0^2 |\langle 2,0 | C_{10} | 1,0 \rangle|^2}{4B_v} \right] \vec{E}; \\ \vec{d}_{1,\pm 1} &= 2 \frac{d_0^2 |\langle 2,\pm 1 | C_{10} | 1,\pm 1 \rangle|^2}{2B_v} \vec{E}. \end{aligned} \quad (8)$$

The induced dipole moment of the $|N, m_N\rangle = |0, 0\rangle$ and $|N, m_N\rangle = |1, \pm 1\rangle$ states have a single contribution from transitions to states with $N' = N + 1$ with larger rotational energies. This leads to a positive dipole moment. For the dipole moment of the $|N, m_N\rangle = |1, 0\rangle$ state contributions from state with both smaller and larger rotational energies appear. In this case their combined effect leads to a negative dipole moment.

V. IMAGINARY PART OF THE POLARIZABILITY

The Hamiltonian described in Section II does not describe losses due to spontaneous emission of rovibrational levels of electronically excited states. These losses appear as an imaginary contribution to the polarizability. We can understand this by realizing that at a specific laser intensity, magnetic and electric field the complex-valued polarizability of state i can also be defined as

$$\alpha(h\nu, \vec{\epsilon}) = \frac{1}{\epsilon_0 c} \sum_f \frac{(E_f - ih\gamma_f/2 - E_i)}{(E_f - ih\gamma_f/2 - E_i)^2 - (h\nu)^2} \times |\langle f | \vec{d}_{tr} \cdot \vec{\epsilon} | i \rangle|^2, \quad (9)$$

where c is the speed of light, ϵ_0 is the electric constant, and kets $|i\rangle$ and $|f\rangle$ denote initial and intermediate rotational-and-hyperfine-resolved vibrational wavefunctions of the $|X^1\Sigma^+\rangle$ potential and excited electronic states. Their energies are E_i and E_f , respectively. The matrix elements $\langle f|\vec{d}_{tr}|i\rangle$ are vibrational-averaged electronic transition dipole moments and $\vec{\epsilon}$ is the polarization of the laser. The sum over f excludes the initial state but includes transitions to the rovibrational levels within the $X^1\Sigma^+$ potential as well as to the rovibrational levels of excited potentials. Contributions from scattering states or the continuum of any state must also be included. For alkali-metal dimers this sum, however, can be limited to transitions to electronic excited potentials that dissociate to either a singly-excited K or Rb atom as only those have significant electronic dipole moments to the $X^1\Sigma^+$ state. Moreover, as we focus on the KRb polarizability for an infrared laser with a 1063 nm wavelength, their contribution is further reduced by the energy denominator in Eq. 9. Finally, the natural line widths γ_f of excited rovibrational levels describe the spontaneous emission that lead to loss of molecules by emission of a spontaneous photon.

As currently only a single measurement of the imaginary part of the polarizability [34] is available to characterize the imaginary part of the two “reduced” polarizabilities of H_{pol} in Eq. 2, we can only compare this $\vec{E} = \vec{0}$ measurement to *ab-initio* theoretical estimates based on Eq. 9. To calculate the theoretical dynamic polarizability we use the most accurate ground state potentials available from Ref. [27]. Excited potentials are constructed from RKR data [28, 29] and as well as from our *ab initio* calculations [30] using long range dispersion coefficients from Ref. [31]. We employ transition dipole moments from our previous electronic structure calculations of KRb [32, 33].

We evaluate the linewidths of excited rovibrational states using two different methods. In the first method, the imaginary part of the polarizability is calculated assuming that the linewidth of rovibrational levels of the $X^1\Sigma^+$ potential is zero and that rovibrational levels of the lowest excited electronic potentials that dissociate to either a singly-excited K or Rb atom, have a natural linewidth equal to the atomic linewidth of potassium. The small, less than 1% difference in linewidth of K and Rb does not modify our results significantly.

For our second method the molecular line width of vibrational levels of potentials that dissociate to either a singly-excited K or Rb atom is calculated assuming an “optical potential” $i\Gamma(r)/2$ [24], where $\Gamma(r)$ is proportional to $\omega(r)^3 d(r)^2$, the frequency $\omega(r)$ is the transition frequency between the two potentials at each r , and $d(r)$ is r -dependent transition dipole moment. This is essentially a stationary phase approximation. The number of electronic potentials included is the same as for the first method.

Figure 7 shows the calculated imaginary part of the polarizability as a function of angle θ for the two means of

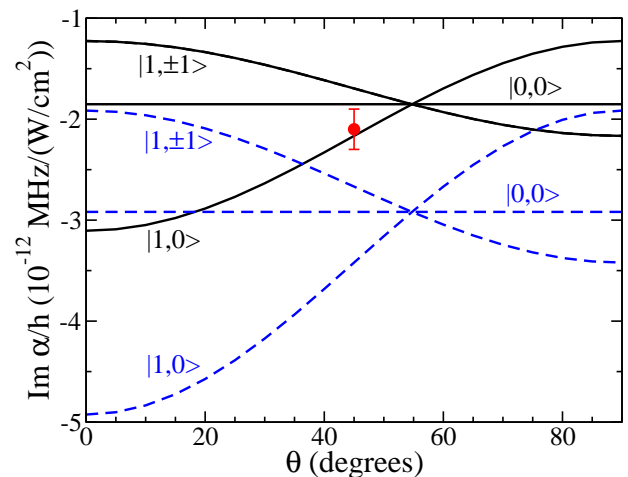


FIG. 7: (Color online) Imaginary part of polarizability of $N = 0$ and 1 rotational levels of the $v = 0$ vibrational level of the $X^1\Sigma^+$ potential of KRb as a function of angle θ between the polarization of the dipole-trap laser at 1063 nm and bias magnetic field with strength $B = 545.9$ G. The static electric field strength is zero. The laser has an intensity of $I = 2.35$ W/cm^2 . Results for two different ways of determining the imaginary polarizability are shown. The solid lines correspond to $\text{Im } \alpha$, when the linewidth of excited ro-vibrational levels equals the atomic linewidth of K, the dashed lines are obtained using excited state linewidths obtained with an “optical potential” approach. The only experimental measurement of the imaginary polarizability for the $|N, m_N\rangle = |0, 0\rangle$ state and $\theta = 45$ degrees [34] is shown by the red marker with error bar.

including the effect of spontaneous emission. The value of the imaginary part is always negative and is seven orders of magnitude smaller than the real part. Eventhough this imaginary part is small, it will affect precision measurements with ultracold KRb molecules. The figure also shows that the absolute value of $\text{Im } \alpha$ is larger for the second method of modeling spontaneous emission. This is because the molecular transition dipole moments from the excited state to the ground state at the equilibrium separation R_e is larger than the atomic dipole moment. The measured $\text{Im } \alpha = -2.1(2) \times 10^{-12}$ $\text{MHz}/(\text{W}/\text{cm}^2)$ for the $|N, m_N\rangle = |0, 0\rangle$ state and $\theta = 45$ degrees [34] is in better agreement with the model that uses the atomic linewidth.

VI. SUMMARY

We performed a theoretical study of the internal rovibronic and hyperfine quantum states of the KRb molecules when simultaneously static magnetic and electric fields as well as trapping lasers are applied. The combined action of these field can be used for an efficient quantum control of ultracold polar molecules in optical potentials. We extended the ideas of mixing rotational

levels in Refs. [18, 23] to include all three fields as in typical ultracold experiments. In particular, we searched for “magic” angles between external DC electric, magnetic, and AC trapping fields, where the AC Stark shift of pairs of rotational states are the same. Moreover, we evaluated the induced dipole moment of the internal rovibronic and hyperfine quantum as a function of external electric field. With this precise value of the dipole moment one can investigate of how interactions between molecules in the different optical lattice sites depend on the relative orientation of the applied fields. Our theoretical research

efforts are closely linked to ongoing experiments with ultracold KRb molecules.

Acknowledgments

We acknowledge funding from Air Force Office of Scientific Research MURI on ultracold polar molecules and the National Science Foundation under grants NSF PHY-1005453 and NSF PHY11-25915.

-
- [1] K.-K. Ni, S. Ospelkaus, M. H. G. de Miranda, A. Pe'er, B. Neyenhuis, J. J. Zirbel, S. Kotochigova, P. S. Julienne, D. S. Jin, and J. Ye, *Science* **322**, 231 (2008).
- [2] S. Ospelkaus, K.-K. Ni, M. H. G. de Miranda, B. Neyenhuis, D. Wang, S. Kotochigova, P. S. Julienne, D. S. Jin, and J. Ye, *Faraday Discuss.* **142**, 361 (2009).
- [3] J. G. Danz, E. Haller, M. Gustavsson, N. Bouloufa, O. Dulieu, H. Ritsch, and H.-C. Nägerl, *Faraday Discuss.* **142** 283 (2009).
- [4] J. G. Danz, M. J. Mark, E. Haller, M. Gustavsson, R. Hart, J. Aldegunde, J. M. Hudson, and H.-C. Nägerl, *Nature Phys.* **6**, 265 (2010).
- [5] S. Ospelkaus, K.-K. Ni, G. Quémener, B. Neyenhuis, M. H. G. de Miranda, J. L. Bohn, J. Ye, and D. S. Jin, *Phys. Rev. Lett.* **104**, 030402 (2010).
- [6] M. H. G. de Miranda, A. Chotia, B. Neyenhuis, D. Wang, G. Quémener, S. Ospelkaus, J. L. Bohn, J. Ye, and D. S. Jin, *Nature Physics* **7**, 502 (2011).
- [7] J. G. Danz, E. Haller, M. Gustavsson, M. J. Mark, R. Hart, N. Bouloufa, O. Dulieu, H. Ritsch, and H.-C. Nägerl, *Science* **321** 1062 (2008).
- [8] M. Baranov, *Phys. Rep.* **464**, 71 (2008).
- [9] T. Lahaye, C. Menotti, L. Santos, M. Lewenstein, and T. Pfau, *Rep. Prog. Phys.* **72**, 126401 (2009).
- [10] D. DeMille, *Phys. Rev. Lett.* **88**, 067901 (2002).
- [11] B. Friedrich and D. Herschbach, *Nature* **353**, 412 (1991).
- [12] J. M. Rost, J. C. Griffin, B. Friedrich, and D. Herschbach, *Phys. Rev. Lett.* **68**, 1299 (1992).
- [13] B. Friedrich and D. Herschbach, *J. Chem. Phys.* **99**, 15686 (1995).
- [14] H. Sakai, S. Minemoto, H. Nanjo, H. Tanji, and T. Suzuki, *Phys. Rev. Lett.* **90**, 083001 (2003).
- [15] J. H. Nielsen, H. Stapelfeldt, J. Küpper, B. Friedrich, J. Omiste, and R. González-Férez, *Phys. Rev. Lett.* **108**, 193001 (2012).
- [16] J. Aldegunde, B. A. Rivington, P. S. Zuchowski, and J. M. Hudson, *Phys. Rev. A* **78**, 033434 (2008).
- [17] J. Aldegunde, H. Ran, and J. M. Hudson, *Phys. Rev. A* **80**, 043410 (2009).
- [18] B. Neyenhuis, B. Yan, S. A. Moses, J. P. Covey, A. Chotia, A. Petrov, S. Kotochigova, J. Ye, and D. S. Jin, *Phys. Rev. Lett.* **109**, 230403 (2012).
- [19] J. Ye, H. J. Kimble, and H. Katori, *Science* **320**, 1734 (2008).
- [20] N. Lundblad, M. Schlosser, and J. V. Porto, *Phys. Rev. A* **81**, 031611(R) (2010).
- [21] A. Derevianko and H. Katori, *Rev. Mod. Phys.* **83**, 331 (2011).
- [22] T. Zelevinsky, S. Kotochigova, and J. Ye, *Phys. Rev. Lett.* **100**, 043201 (2008).
- [23] S. Kotochigova and D. DeMille, *Phys. Rev. A* **82**, 063421 (2010).
- [24] B. Zygelman and A. Dalgarno, *Phys. Rev. A* **38**, 1877 (1988).
- [25] D. M. Brink and G. R. Satchler, *Angular Momentum*, 3rd ed. (Clarendon Press, Oxford, 1993).
- [26] E. Arimondo, M. Inguscio, and P. Violoni, *Rev. Mod. Phys.* **49**, 31 (1977).
- [27] A. Pashov, O. Docenko, M. Tamanis, R. Ferber, H. Knöckel, and E. Tiemann, *Phys. Rev. A* **76**, 022511 (2007).
- [28] S. Kasahara, C. Fujiwara, N. Okada, and H. Katô, *J. Chem. Phys.* **111**, 8857 (1999).
- [29] C. Amiot, *J. Mol. Spect.* **203**, 126 (2000).
- [30] S. Kotochigova, E. Tiesinga, and P. S. Julienne, *New J. Phys.* **11**, 055043 (2009).
- [31] B. Busser, Y. Achkar, and M. Aubert-Fréçon, *Chem. Phys.* **116**, 319 (1987).
- [32] S. Kotochigova, P. S. Julienne, and E. Tiesinga, *Phys. Rev. A* **68**, 022501 (2003).
- [33] S. Kotochigova, E. Tiesinga, and P. S. Julienne, *Eur. Phys. J. D* **31**, 189 (2004).
- [34] A. Chotia, B. Neyenhuis, S. A. Moses, B. Yan, J. P. Covey, M. Foss-Feig, A. M. Rey, and J. Ye, *Phys. Rev. Lett.* **108**, 080405 (2012).